

Mechanisms for Abrupt Summertime Circumpolar Surface Warming in the Southern Ocean

EARLE A. WILSON,^a DAVID B. BONAN,^b ANDREW F. THOMPSON,^b NATALIE ARMSTRONG,^c AND STEPHEN C. RISER^d

^a *Department of Earth System Science, Stanford University, Stanford, California*

^b *Environmental Science and Engineering, California Institute of Technology, Pasadena, California*

^c *Department of Environmental Health and Engineering, The Johns Hopkins University, Baltimore, Maryland*

^d *School of Oceanography, University of Washington, Seattle, Washington*

(Manuscript received 6 July 2022, in final form 16 June 2023, accepted 27 June 2023)

ABSTRACT: In recent years, the Southern Ocean has experienced unprecedented surface warming and sea ice loss—a stark reversal of the sea ice expansion and surface cooling that prevailed over the preceding decades. Here, we examine the mechanisms that led to the abrupt circumpolar surface warming events that occurred in late 2016 and 2019 and assess the role of internal climate variability. A mixed layer heat budget analysis reveals that these recent circumpolar surface warming events were triggered by a weakening of the circumpolar westerlies, which decreased northward Ekman transport and accelerated the seasonal shoaling of the mixed layer. We emphasize the underappreciated effect of the latter mechanism, which played a dominant role and amplified the warming effect of air–sea heat fluxes during months of peak solar insolation. An examination of the CESM1 large ensemble demonstrates that these recent circumpolar warming events are consistent with the internal variability associated with the Southern Annular Mode (SAM), whereby negative SAM in austral spring favors shallower mixed layers and anomalously high summertime SST. A key insight from this analysis is that the seasonal phasing of springtime mixed layer depth shoaling is an important contributor to summertime SST variability in the Southern Ocean. Thus, future Southern Ocean summertime SST extremes will depend on the coevolution of mixed layer depth and surface wind variability.

SIGNIFICANCE STATEMENT: This study examines how reductions in the strength of the circumpolar westerlies can produce abrupt and extreme surface warming across the Southern Ocean. A key insight is that the mixed layer temperature is most sensitive to surface wind perturbations in late austral spring, when the regional mixed layer depth and solar insolation approach their respective seasonal minimum and maximum. This heightened surface temperature response to surface wind variability was realized during the austral spring of 2016 and 2019, when a dramatic weakening of the circumpolar westerlies triggered unprecedented warming across the Southern Ocean. In both cases, the anomalously weak circumpolar winds reduced the northward Ekman transport of cool subpolar waters and caused the mixed layer to shoal more rapidly in the spring, with the latter mechanism being more dominant. Using results from an ensemble of coupled climate simulations, we demonstrate that the 2016 and 2019 Southern Ocean warming events are consistent with the internal variability associated with the Southern Annular Mode (SAM). These results suggest that future Southern Ocean surface warming extremes will depend on both the evolution of regional mixed layer depths and interannual wind variability.


KEYWORDS: Southern Ocean; Ocean dynamics; Extreme events; Mixed layer; Climate variability; Subseasonal variability

1. Introduction

The Southern Ocean has experienced exceptional sea ice decline and surface warming in recent years (Fig. 1). During the austral spring of 2016, Antarctic sea ice retreated at an unusually rapid rate before reaching a record-low extent the following summer (Turner et al. 2017; Parkinson 2019; Eays et al. 2021). This anomalous sea ice decline coincided with widespread surface warming that extended beyond the Antarctic sea ice zone and culminated in record-high summertime

sea surface temperatures (SSTs; Stuecker et al. 2017; Meehl et al. 2019, Fig. 1a). While Southern Ocean SSTs returned to normal after a few months, Antarctic sea ice extent (SIE) remained exceptionally low over the next three years. In late 2019, the Southern Ocean experienced another abrupt circumpolar surface warming event of similar magnitude and spatial extent as the anomalous warming of late 2016, but there was no corresponding decline in Antarctic SIE (Fig. 1b).

The extent to which these recent warming and sea ice loss anomalies reflect a shift in the Southern Ocean climate or transient manifestations of internal variability remains unclear. Over the preceding decades, the Southern Ocean experienced robust sea ice expansion and surface cooling that were near circumpolar in extent (Yuan and Martinson 2000; Cavalieri et al. 2003; Simmonds 2015). The underlying drivers

 Denotes content that is immediately available upon publication as open access.

Corresponding author: Earle A. Wilson, earlew@stanford.edu

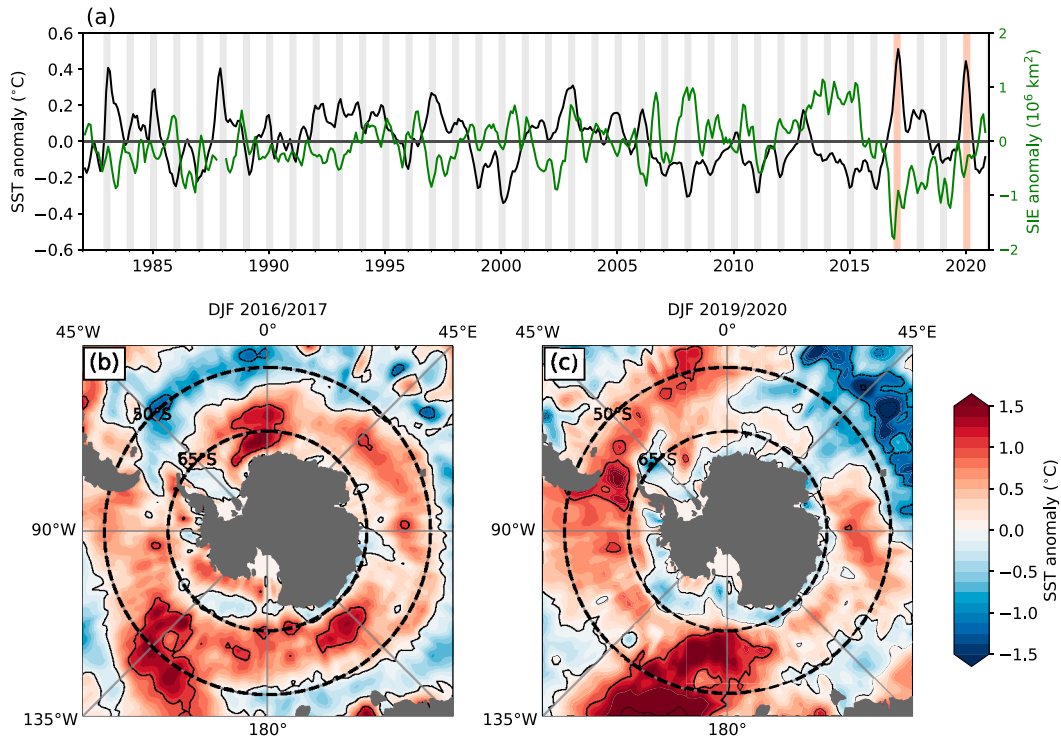


FIG. 1. (a) Temporal evolution of monthly anomalies in SST (black) and Antarctic SIE (green) in the Southern Ocean. (b),(c) Seasonally averaged maps of anomalous SST during December–February (DJF) of 2016/17 and 2019/20. In (a), the vertical gray bars highlight austral summer (December–February). Dashed lines in (b) and (c) highlight 50°–65°S, the latitudes over which the SST anomalies are spatially averaged in (a). Each time series has been smoothed with a 3-month rolling average.

of these longer time scale trends are uncertain. Possible mechanisms include the strengthening of the circumpolar westerlies (Fan et al. 2014; Kostov et al. 2017), increases in surface freshwater fluxes and stratification (Bintanja et al. 2013; Purich et al. 2018; Haumann et al. 2020), atmospheric teleconnections from the tropical Pacific (Meehl et al. 2016; Li et al. 2021; Chung et al. 2022), and internal climate variability associated with Weddell Sea deep convection (Zhang et al. 2019). While increased greenhouse gas emissions will eventually lead to sustained warming and sea ice loss across the Southern Ocean (Ferreira et al. 2015; Armour et al. 2016; Kostov et al. 2017), the time scale over which an anthropogenic signal will emerge above the noise of internal variability is poorly constrained (Holland et al. 2017; Doddridge et al. 2019; Rackow et al. 2022).

Previous studies suggest that the anomalous decline in Antarctic SIE that began in 2016 was due to multiple mechanisms operating over various time scales. The initial sea ice loss has been linked to anomalous variations in the Southern Annular Mode (SAM), El Niño–Southern Oscillation (ENSO), and the Indian Ocean dipole (IOD), which collectively weakened the circumpolar westerly jet and facilitated anomalous poleward advection of warm subtropical air into the subpolar region (Stuecker et al. 2017; Schlosser et al. 2018; Wang et al. 2019; Purich and England 2019). These mechanisms are distinct from the enhanced upwelling of warm Circumpolar

Deep Water (CDW) that is expected to drive Southern Ocean sea ice loss and surface warming over the next century (Bitz and Polvani 2012; Ferreira et al. 2015). However, a gradual build-up of subsurface heat in the seasonal sea ice zone may have preconditioned some areas of the Southern Ocean for an unusually rapid springtime retreat of Antarctic sea ice (Meehl et al. 2019; Campbell et al. 2019; Zhang et al. 2022).

It is possible that the mechanisms responsible for the recent decline in Antarctic sea ice are related but distinct from those that led to the recent circumpolar surface warming events. Although the 2016 surface warming coincided with a steep loss in Antarctic sea ice, this was not the case in late 2019 (Fig. 1a). Furthermore, previous circumpolar surface warming events, such as those that occurred during the austral spring and summers of 1982/83 and 1987/88, were not accompanied by an appreciable decrease in Antarctic SIE (Fig. 1a). As with the late 2016 and 2019 warming events, these earlier circumpolar warming events extended beyond the seasonal sea ice zone. Though previous studies have established links between Southern Ocean SST anomalies and the variability of SAM and ENSO (Sen Gupta and England 2006; Sallée et al. 2010; Ciasto and England 2011; Ding et al. 2012; Doddridge and Marshall 2017), there is no clear relationship between the intensity of SAM or ENSO phases and the magnitude of Southern Ocean SST anomalies. Thus, the particular set of circumstances that facilitated the extraordinary summertime SST anomalies in 2016/17 and 2019/20 remain unclear.

Since these surface warming events occur in spring and summer, they help set the upper bound on near-surface temperatures in the Southern Ocean. Critically, circumpolar warming events may provide the basis for marine heatwaves (MHWs), which are more localized SST extremes that can lead to sharp declines in biodiversity and the collapse of ecosystems (Hobday et al. 2016; Frölicher et al. 2018; Holbrook et al. 2019; Smale et al. 2019; Oliver et al. 2021). Moreover, these severe warm events enhance upper ocean stratification, which affects vertical mixing and air–sea gas exchange. Therefore, understanding the mechanisms that may lead to surface warming extremes is an essential step toward characterizing and predicting ecological sustainability in the Southern Ocean.

The primary purpose of this work is to elucidate the large-scale atmospheric and oceanic processes that give rise to extreme and abrupt circumpolar surface warming across the Southern Ocean. This work builds on previous analyses that have examined the seasonal evolution of Southern Ocean mixed layer temperature (MLT; Dong et al. 2007, 2008; Tamsitt et al. 2016; Pellichero et al. 2017) by focusing on processes that can lead to severe surface warming during summer months. Likewise, our analysis extends previous work that has explored the Southern Ocean response to SAM and ENSO (Sen Gupta and England 2006; Sallée et al. 2010; Ciasto and England 2011) by explicitly examining how the seasonal phasing of these modes of climate variability can produce extreme summertime SSTs. In doing so, we assess the extent to which recent circumpolar surface warming anomalies can be explained by internal variability. A key result of this analysis is that variations in the seasonal phasing of mixed layer depth (MLD) and solar insolation during austral spring are important contributors to the interannual variability in Southern Ocean summertime SST.

2. Data and methods

a. Observations and reanalyses

Monthly SST data were obtained from the NOAA Optimum Interpolation (OI) SST V2 product (Reynolds et al. 2002), while subsurface temperature and salinity variability were computed from the Argo-based Roemmich–Gilson climatology (Roemmich and Gilson 2009). Estimates of Antarctic sea ice concentration (SIC) were retrieved from the NOAA/NSIDC Climate Data Record (CDR) of SIC (Meier et al. 2021). SIE is defined as the area over which SIC is greater than 15%. Estimates of surface wind stress, sea level pressure, and air–sea heat fluxes were sourced from the ECMWF monthly ERA5 global atmospheric reanalysis, which were provided on a $0.25^\circ \times 0.25^\circ$ horizontal grid (Hersbach et al. 2020). The reanalysis estimates were remapped to a coarser $1^\circ \times 1^\circ$ horizontal grid using a bilinear interpolation scheme to be consistent with the RG Argo and the NOAA OI SST data products.

While the SST data and atmospheric reanalysis products are analyzed for 1982–2020, the mixed layer heat budget analysis is carried out for the 2004–20 period when subsurface Argo data are available. MLD is defined as the depth where potential density is 0.03 kg m^{-3} greater than its value at the surface (de Boyer Montégut et al. 2004). The SAM

index is defined as the zonal-mean sea level pressure difference between 65° and 40°S (Marshall 2003). ENSO variability is quantified using the Niño-3.4 index, which describes the area-averaged SST anomaly between $170^\circ\text{--}120^\circ\text{W}$ and $5^\circ\text{S--}5^\circ\text{N}$. The SAM and Niño-3.4 indices are normalized by their respective standard deviations. Anomalies are computed relative to a monthly averaged climatology. For the SST and reanalysis data, the climatological reference period is 1982–2015, whereas for the Argo data the climatological reference period is 2004–15.

To contextualize recent abrupt circumpolar warming events, observations are compared with output from the Community Earth System Model Version 1 Large Ensemble (CESM1-LE; Kay et al. 2015). The CESM1-LE is a fully coupled, 1° horizontal resolution, 40-member initial condition ensemble, where each ensemble member is subjected to identical historical and RCP8.5 external forcing scenarios. Each member differs slightly in its initial atmospheric state, producing a representation of internal variability across ensemble members, in the presence of forced climate change. The CESM1-LE includes the Community Atmosphere Model version (CAM5; Hurrell et al. 2013) and the Parallel Ocean Program version 2 (POP2; Danabasoglu et al. 2012). POP2 employs the *K*-profile parameterization (KPP) vertical mixing scheme and a mixed layer eddy parameterization to capture the restratifying effect of submesoscale baroclinic eddies (Fox-Kemper et al. 2008). We focus on model output from the 1980–2020 period that overlaps with the modern satellite record.

The CESM1-LE generates SAM and ENSO variability that compares well with observations. In particular, the ensemble experiment robustly captures the positive trend in SAM during austral summer that has been observed over the satellite era (Holland et al. 2017). The CESM1-LE also generates realistic seasonality of ENSO, but slightly overestimates its magnitude (Zheng et al. 2018). Like many other state-of-the-art climate models, CESM1-LE suffers from a shallow bias in mixed layer depth for some regions of the Southern Ocean (Danabasoglu et al. 2012; Sallée et al. 2013; Huang et al. 2014), which would favor stronger MLT responses to changes in surface forcing.

b. Southern Ocean mixed layer heat budget

The physical controls on Southern Ocean SST are evaluated using a mixed layer heat budget. Here, MLT and SST are assumed to be equivalent. The heat budget is constructed for the mostly ice-free latitude band of $50^\circ\text{--}65^\circ\text{S}$, which envelops the core of the circumpolar westerly jet and much of the Antarctic Circumpolar Current (ACC). This is the latitudinal band over which SAM induces surface cooling during its positive phase and surface warming during its negative phase (Sen Gupta and England 2006); farther north, between 30° and 50°S , the SST response to SAM is reversed. This analysis focuses on surface temperature variability across the circumpolar band of $50^\circ\text{--}65^\circ\text{S}$ since the anomalous warming events of late 2016 and 2019 were most pronounced across these latitudes (see Figs. 1b,c).

As demonstrated by Dong et al. (2007), domain-averaged variations in MLT (T_m) across the circumpolar channel is primarily governed by heating due to air–sea fluxes, northward Ekman transport, and wind-driven entrainment. This balance is given by

$$\frac{1}{A_s} \iint \frac{\partial T_m}{\partial t} dA \approx \frac{1}{A_s} \iint \left(\frac{Q_{ao}}{\rho_0 c_w h_m} - v_{Ek} \frac{\partial T_m}{\partial y} - w_{ent} \frac{\Delta T}{h_m} \right) dA, \quad (1)$$

$$\frac{1}{A_s} \iint \dot{T}_m dA \approx \frac{1}{A_s} \iint (\dot{T}_{ao} - \dot{T}_{Ek} - \dot{T}_{ent}) dA, \quad (2)$$

$$\dot{\bar{T}}_m \approx \dot{\bar{T}}_{ao} - \dot{\bar{T}}_{Ek} - \dot{\bar{T}}_{ent}, \quad (3)$$

where Q_{ao} is the net air–sea heat flux due to the sum of radiative and turbulent heat fluxes, v_{Ek} is the meridional Ekman velocity, ΔT is the temperature difference between the mixed layer and 10 m below the mixed layer, c_w is the specific heat capacity of seawater, h_m is the mixed layer depth, $w_{ent} = \dot{h}_m$ is the entrainment rate, and A_s is the surface area of the circumpolar control volume. Here, the dot and overbar symbolize temporal tendency and spatial averages, respectively. The meridional Ekman velocity is given by $v_{Ek} = \tau^x / (\rho_0 f h_m)$, where τ^x is the zonal component of the surface wind stress, $\rho_0 = 1025 \text{ kg m}^{-3}$ is a reference seawater density, and $f \approx 10^{-4} \text{ s}^{-1}$ is the Coriolis parameter. Following the procedure outlined in Dong et al. (2007), Q_{ao} is modified slightly to account for the fraction of shortwave radiation that is transmitted through the base of the mixed layer.

Equation (3) is valid when evaluating the heat balance over the entire circumpolar channel. On smaller spatial scales, geostrophic transport and eddy mixing, which are neglected in this framework, have leading-order impacts on surface temperature variability (Tamsitt et al. 2016; du Plessis et al. 2022; Gao et al. 2022). It is also assumed that meridional eddy fluxes across the northern and southern boundaries of the control volume make small contributions to the domain-averaged MLT tendency $\dot{\bar{T}}_m$ on monthly time scales. Compared to the terms in Eq. (2), the domain-averaged contribution of Ekman pumping on the mixed layer heat budget is negligibly small on monthly time scales. Although it is relatively straightforward to evaluate $\dot{\bar{T}}_{ao}$ and $\dot{\bar{T}}_{Ek}$ from Argo data and atmospheric reanalysis, $\dot{\bar{T}}_{ent}$ presents a greater challenge since it is influenced by submonthly variations in h_m that are not well resolved by the current Argo observing array (Carranza and Gille 2015). Therefore, the effect of vertical entrainment is estimated from the residual of the other heat budget terms. While other processes, such as submesoscale mixing and meridional geostrophic advection, as well as measurement errors may contribute to the residual, we expect the effect of vertical mixing to be dominant. Vertical entrainment will have a cooling effect in the summer when the warm mixed layer overlies the cool remnants of the winter mixed layer and a slight warming effect in the winter when the cold, deep mixed layer is in contact with the relatively warm Circumpolar Deep Water (Dong et al. 2007).

3. Results

a. Environmental conditions during the late 2016 and 2019 Southern Ocean warming events

During the austral spring of 2016 and 2019, the domain-averaged surface buoyancy fluxes across the Southern Ocean were not consistently different from the climatological mean (Fig. 2a). Although the late 2016 warming event followed unusually warm winter and spring, this was not the case in 2019. Additionally, the spatial patterns of anomalous air–sea fluxes were not consistent with the patterns of anomalous warming during both circumpolar warming events (Fig. 3). While in some instances, patterns of anomalous air–sea heating and mixed layer warming overlapped, this was often not the case. For example, during November–January of 2019, air–sea heat fluxes across the southern Atlantic favored anomalous surface cooling while the mixed layer warmed at an accelerated rate (Figs. 3e,f). Thus, anomalous air–sea heating cannot entirely explain these recent circumpolar warming events.

On the other hand, circumpolar westerlies were extraordinarily weak in late 2016 and 2019, with zonally averaged surface wind stress anomalies exceeding -0.04 N m^{-2} (Fig. 2b)—a $\sim 30\%$ reduction relative to the climatological mean. During both warming events, the collapse of the surface westerlies spanned all longitudes (Figs. 3c,h). Concurrently, there was widespread anomalous MLD shoaling across the Southern Ocean (Figs. 3d,i). The anomalous shoaling was most striking in late 2019 when the MLD across the circumpolar channel was, on average, roughly 20% shallower than usual. The late 2016 and 2019 anomalous shoaling events did not coincide with increased surface heat or freshwater fluxes (Fig. 2a).

Consistent with the strong reduction in circumpolar westerly winds, SAM was in an exceptionally negative phase during both circumpolar warming events. In both cases, the SAM index was roughly 1.5 standard deviations below its annual mean value (Fig. 2c). ENSO was in a relatively neutral state during these periods, tending toward its La Niña- and El Niño-like states during the austral spring of 2016 and 2019, respectively.

b. Drivers of anomalous mixed layer warming in late 2016 and 2019

Evaluating the circumpolar mixed layer heat budget [Eq. (3)] reveals that the anomalous surface warming in late 2016 and 2019 were primarily caused by heating anomalies associated with air–sea heat fluxes $\dot{\bar{T}}_{ao}$ and northward Ekman transport $\dot{\bar{T}}_{Ek}$ (Fig. 4). In late 2016, $\dot{\bar{T}}_{Ek}$ anomalies peaked at roughly $0.08^\circ\text{C month}^{-1}$, which was slightly less than the overall mixed layer warming of $0.1^\circ\text{C month}^{-1}$ (Fig. 4b). In late 2019, anomalies in $\dot{\bar{T}}_{Ek}$ accounted for roughly half of the observed mixed layer warming. The decrease in Ekman-driven cooling is consistent with the anomalously weak zonal wind stress during these periods (Figs. 3c,h). As discussed in the preceding section, the increase in $\dot{\bar{T}}_{ao}$ cannot be entirely explained by enhanced air–sea heat fluxes since these fluxes were not substantially different from the climatology during both warming events (Fig. 2b). This implies that the amplified effect of $\dot{\bar{T}}_{ao}$ was largely due to the

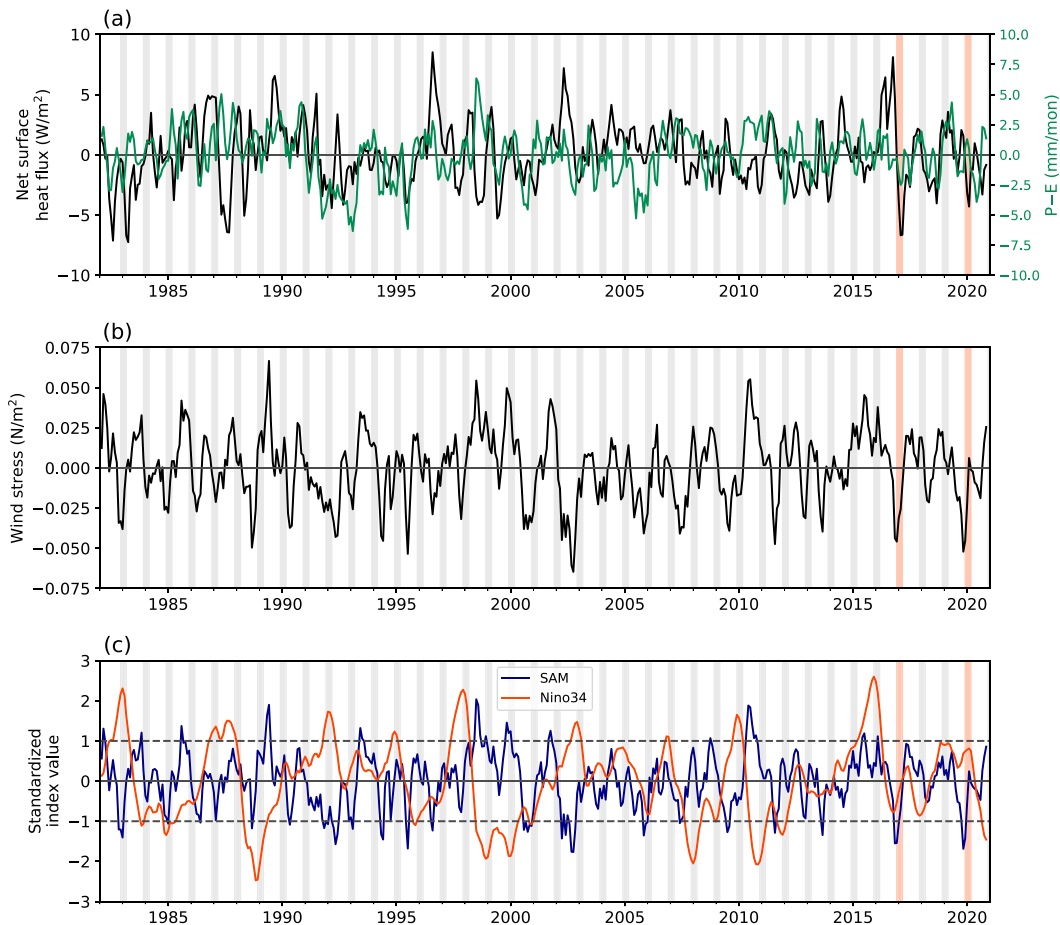


FIG. 2. (a) Domain-averaged net surface heat flux anomalies (black) and precipitation minus evaporation anomalies ($P - E$, green) across 50° – 65° S. Positive air–sea heat fluxes signify ocean heat gain. (b) As in (a), but showing zonal wind stress anomalies. (c) Temporal evolution of the SAM (blue) and the Niño-3.4 indices (orange). Vertical gray bars highlight austral summer (December–February). The linear trend has been removed from each time series, and temporal variations are smoothed using a 3-month rolling average.

anomalous shoaling of the mixed layer (Figs. 3d,i). When \bar{T}_{ao} is computed using climatological MLDs (purple line in Fig. 2b), its contribution to the 2016 and 2019 warming events is substantially reduced. For the latter event, \bar{T}_{ao} is reduced by an order of magnitude and accounts for less than 20% of the observed warming anomaly when the effect of MLD shoaling is removed.

The evolution of the residual of Eq. (3) suggests that the entrainment-driven mixed layer cooling was enhanced during late 2016 and 2019 (Fig. 4b). In absolute terms, this represents an increase in the entrainment-driven cooling that typically occurs in summer months (Fig. 4a). The implied amplification of \bar{T}_{ent} under weaker surface winds suggests a complex interplay between wind-driven mixing, MLD, and the variance of surface winds. Since \bar{T}_{ent} is dependent on MLD and the temperature gradient below the mixed layer [Eq. (3)], this term does not necessarily scale with the amplitude of the surface wind stress. Moreover, the temperature of a shallower mixed layer will be more sensitive to the mixing generated by episodic storms and strong wind events. Nevertheless, without

direct estimates of entrainment-driving mixing, the contribution of \bar{T}_{ent} is not well constrained.

c. The seasonal phasing of mixed layer depth and air–sea heat fluxes

The heat budget analysis suggests that the abrupt surface warming events in late 2016 and 2019 were triggered by a weakening of the circumpolar westerlies and a concurrent shoaling of the mixed layer. In the subsequent section, we demonstrate that the latter effect resulted directly from weaker surface winds. Although the surface wind anomalies were relatively large during the warming events, the amplitude of these anomalies was not unprecedented (Fig. 2b). The discrepancies between the relative magnitudes of the surface wind anomalies and concurrent MLT anomalies in late 2016 and 2019 suggest other factors were at play.

To explore the effect of the seasonal phasing of surface wind, MLD, and MLT anomalies, we reexamine the seasonal evolution of \bar{T}_m in the phase space defined by h_m and Q_{ao}

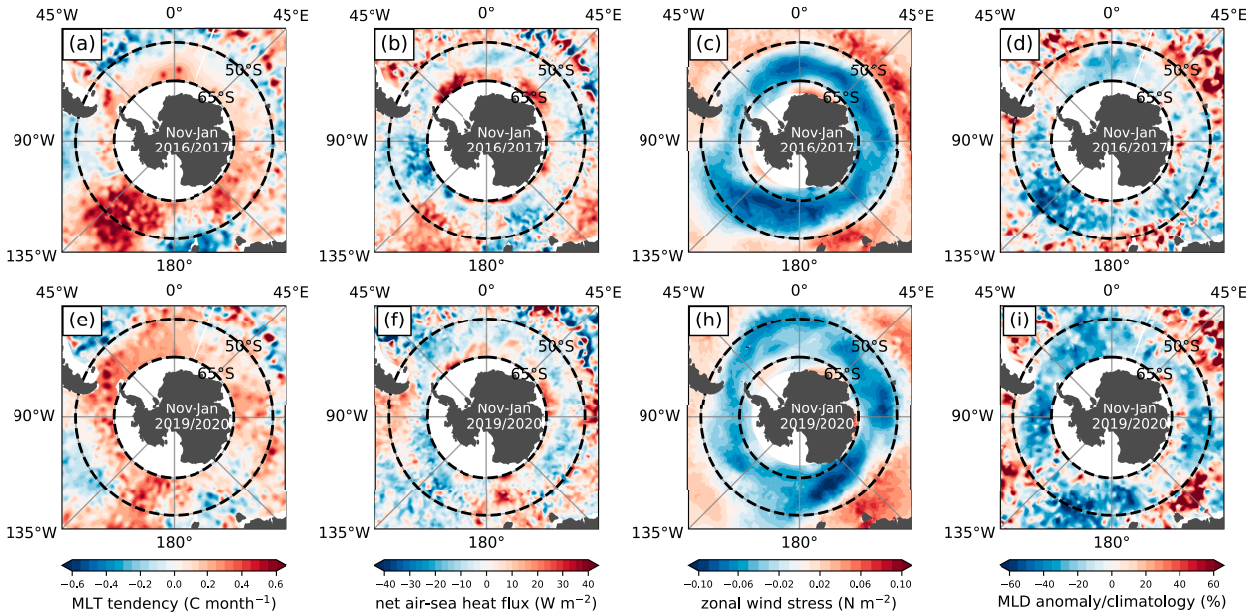


FIG. 3. Southern Ocean surface conditions during November–January of (top) 2016 and (bottom) 2019: (a),(e) MLT tendency anomalies, (b),(f) net air–sea heat flux anomalies, (c),(g) zonal wind stress anomalies, and (d),(i) MLD anomalies as percentages of the monthly climatological means. Black dashed lines outline the circumpolar channel (50° – 65° S) over which the mixed layer heat budget is evaluated. Since the MLD appears in the denominator of the heat budget terms [Eq. (1)], we show the fractional change rather than the absolute anomalies.

(Fig. 5). Since the seasonal variation of τ^x is small compared to that of MLD and Q_{ao} , we focus on the sum of the mixed layer warming due to northward Ekman transport and air–sea heat fluxes, $\bar{T}_{ao+Ek} \equiv \bar{T}_{ao} + \bar{T}_{Ek}$, assuming a constant surface wind stress of $\tau^x = 0.15 \text{ N m}^{-2}$. During the cooling season (March–September), \bar{T}_{ao} and \bar{T}_{Ek} combine to cool the relatively deep mixed layer at a peak rate of approximately $0.75^{\circ}\text{C month}^{-1}$. During the warming season (October–February), \bar{T}_{ao+Ek} provides a surface warming that reaches a maximum of $\sim 2^{\circ}\text{C month}^{-1}$ between January and February. The seasonal asymmetry of \bar{T}_{ao+Ek} arises from the nonlinear dependence of \bar{T}_{ao} on h_m . As h_m approaches its summertime minimum, \bar{T}_{ao+Ek} becomes increasingly sensitive to variations in h_m and Q_{ao} , with \bar{T}_{ao} being more sensitive to periods of anomalous mixed layer shoaling than anomalous deepening. The effect of \bar{T}_{Ek} may be discerned by the offset in the position of the $\bar{T}_{ao+Ek} = 0$ contour in Fig. 5; the transect across $Q_{ao} = 0$ quantifies the cooling due to northward Ekman transport.

In the phase space defined by h_m and Q_{ao} , the impact of the extraordinary MLD shoaling in late 2016 and 2019 is immediately evident. During these anomalous warming periods (green lines in Fig. 5), the Southern Ocean mixed layer followed a relatively shallow trajectory in the Q_{ao} – h_m phase space, which accelerated the springtime warming of the mixed layer. In most years, Q_{ao} reaches a maximum amplitude of $\sim 150 \text{ W m}^{-2}$ in December, one month before h_m reaches its minimum value of $\sim 40 \text{ m}$. In late 2016 and 2019, the seasonal h_m minimum occurred approximately one month earlier than usual, coinciding with maximal air–sea heat fluxes. This shoaling-induced mixed

layer warming anomaly was most apparent in November of 2019 when h_m was 20–30 m shallower than the climatological mean—a record low for the Argo period. The enhanced mixed layer warming due to \bar{T}_{ao} is augmented by a reduction in the cooling provided by \bar{T}_{Ek} , which equates to a downward translation of the \bar{T}_{ao+Ek} pattern in Fig. 5. The accelerated mixed layer warming of late 2016 and 2019, which occurred during strong negative SAM events, is contrasted with the more gradual warming that occurred in late 2010 (purple line in Fig. 5), a period characterized by positive SAM conditions (Figs. 2b,c). In the latter scenario, the anomalously deep Southern Ocean mixed layer warmed at a relatively slow rate, leading to anomalously cool summertime surface temperatures (Fig. 1a).

d. Sensitivity of mixed layer warming to the timing of surface wind anomalies

The preceding analyses suggest that a weakening of the circumpolar westerlies during the austral spring of 2016 and 2019 initiated anomalous mixed layer shoaling and that the unusual timing of these anomalies led to extreme surface warming. This mechanism is explored further using a set of idealized mixed layer simulations. We employ a one-dimensional Kraus–Turner mixed layer model (Kraus and Turner 1967) that evolves MLD in response to surface momentum and buoyancy fluxes (appendix). The Kraus–Turner model is augmented to account for the effect of lateral Ekman transport using the formulation discussed in section 2b, using the annual-mean meridional temperature gradient of $4.5 \times 10^{-6} \text{ }^{\circ}\text{C m}^{-1}$. The numerical model is evolved with a vertical resolution of 1 m and a 6-hourly time step.

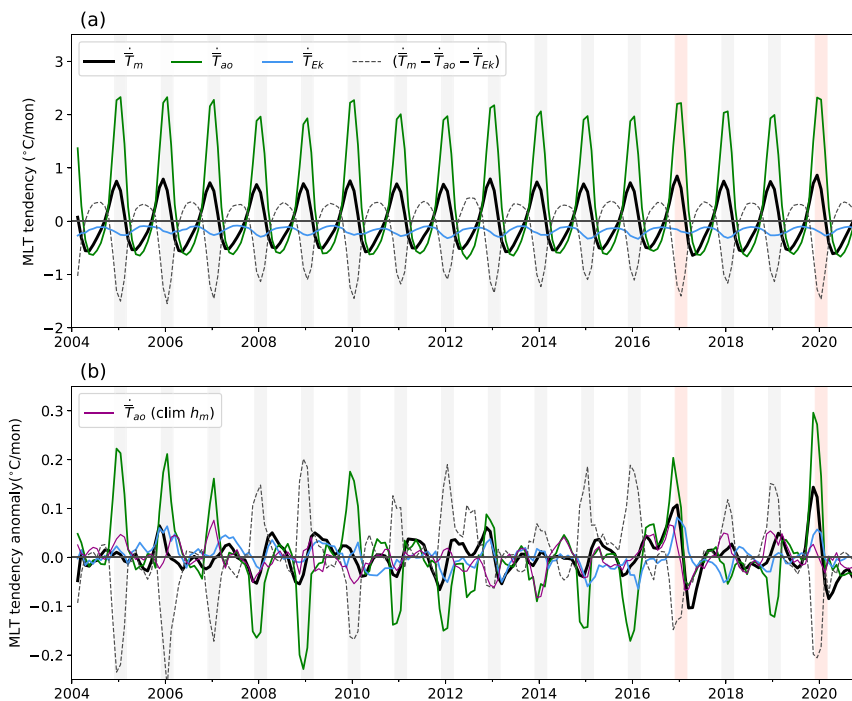


FIG. 4. Evolution of the Southern Ocean mixed layer heat budget, described by Eq. (3). (a) Monthly tendencies in MLT (black) due to air–sea heat fluxes (green) and meridional Ekman transport (blue). The gray dashed line represents the residual of the heat budget ($\dot{T}_m - \dot{T}_{ao} - \dot{T}_{Ek}$), which is interpreted as the component due to entrainment. (b) As in (a), but after removing the monthly climatology. Gray vertical bars highlight December–February. The purple line in (b) represents monthly \dot{T}_{ao} anomalies computed using climatological mixed layer depth.

The mixed layer model was forced with idealized surface fluxes of buoyancy and momentum that resemble observations across 50° – 65° S during October and February (see the appendix). We prescribe a surface heat flux and wind stress using climatological monthly mean values from ERA5 reanalysis. To account for sub-monthly wind variability, we superimpose onto the climatological forcing randomly generated values sampled from a red-noise spectrum, with a standard deviation of 0.15 N m^{-2} . To obtain robust results, 500 simulations were conducted, each with a unique wind stress forcing. Increasing the ensemble size does not substantially change the main results. For simplicity, we impose a constant surface freshwater flux of 4 mm day^{-1} , which is roughly equivalent to the annual mean freshwater flux across the circumpolar channel (Abernathey et al. 2016).

For the perturbation experiments, a Gaussian kernel is used to reduce the wind stress magnitude by a maximum value of 50% over a 10-day window while preserving the temporal variance. The wind anomalies were applied independently to each month between October and March to generate five independent perturbation experiments.

For the reference case, the mixed layer gradually shoals and warms between October and February, reaching a minimum depth of roughly 50 m and a maximum temperature of approximately 3.5°C , which are consistent with observations (Fig. 6). Reducing the strength of the wind causes the mixed layer to shoal and warm. The amplitude of the MLD ranges

between 5 and 20 m and is not sensitive to the timing of the wind anomaly. In contrast, the MLT response varies substantially with the timing of the wind perturbation. When the wind perturbation is applied in October, the anomalously shallow mixed layer experiences negligible warming ($<0.01^{\circ}\text{C}$) as the surface heat fluxes are weak and the MLD is relatively deep during this month. However, similar wind perturbations during November and February lead to substantially larger MLT anomalies, ranging between 0.05° and 0.2°C . A large fraction of the MLT anomaly persists after the wind perturbation as less heat is mixed down to deeper layers compared to the reference case. These MLT anomalies eventually dissipate when the mixed layer deepens in fall and winter (not shown). Weaker winds also lead to an increase in entrainment-driven mixed layer cooling \dot{T}_{ent} , which is consistent with what is inferred from observations in late 2016 and 2019 (Fig. 4).

To better represent the observed warming events in late 2016 and 2019, we conduct an additional set of mixing experiments with a more prolonged period of reduced surface wind stress, spanning October through December (Fig. 7). Even though this numerical experiment is highly idealized, it captures the timing and magnitude of the ML shoaling and warming of late 2016 and 2019 remarkably well. Similar to observations, the simulated shoaling coincides with the wind perturbation while the warming lags by 1–2 months (Figs. 7d,f). While weaker winds reduce the Ekman cooling, the main driver of the warming is

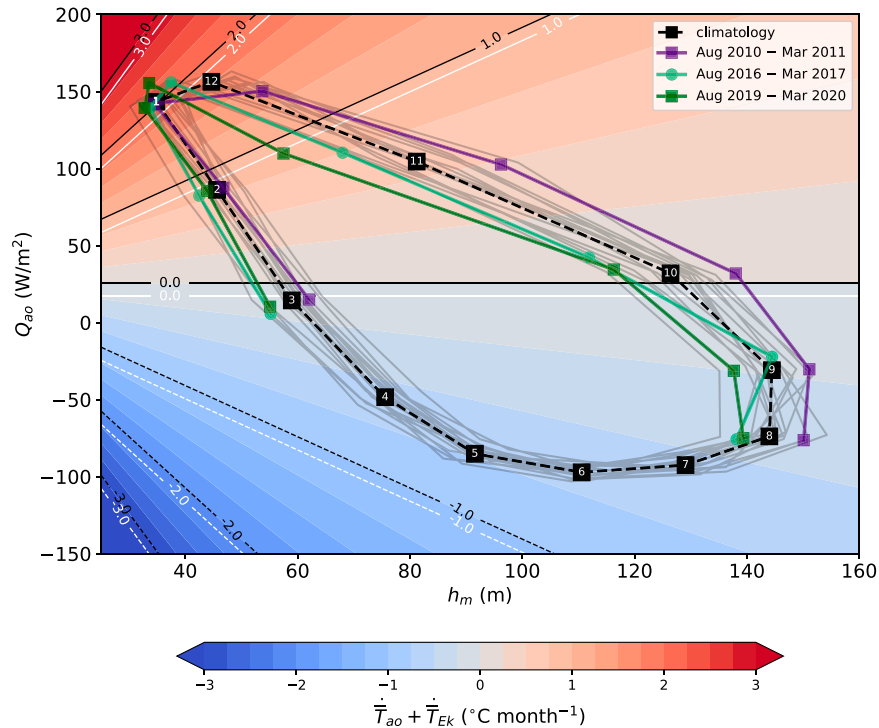


FIG. 5. Phase diagram showing the relationship between seasonal variations in mixed layer depth h_m , air-sea heat fluxes Q_{ao} , and mixed layer temperature tendency due to the sum of air-sea heating \bar{T}_{ao} and Ekman transport \bar{T}_{Ek} (contours and shading). Gray lines represent seasonal trajectories from 2004 to 2020, while the dashed black line represents the climatological mean. For the latter, the numbering of the black squares signifies the calendar month. The green lines highlight trajectories between August–March in 2016/17 and 2019/20 when SAM was in a negative phase during austral spring. Conversely, the purple line highlights an equivalent trajectory in 2010/11 when the SAM was in a positive phase. For the background shading and black contours, the heating associated with northward Ekman transport \bar{T}_{Ek} is computed assuming a typical value of $\tau^x = 0.15\ N\ m^{-2}$. White contours show $\bar{T}_{ao} + \bar{T}_{Ek}$ for the case where $\tau^x = 0.1\ N\ m^{-2}$.

MLD shoaling. Additional experiments with the Ekman transport turned off produce similar results, albeit with warmer mean MLTs and slightly smaller time-mean MLT anomalies. The strong correspondence between the idealized simulations and observations bolsters the hypothesis that anomalous wind-driven mixed layer shoaling in spring can lead to exceptional surface warming in the summer.

e. Role of internal climate variability

To ascertain the potential role of internal climate variability in these recent surface warming events, we examine output from the 40-member CESM1-LE to gain a more robust understanding of these phenomena. Specifically, we investigate the response of summertime [December–February (DJF)] Southern Ocean SST to variations of SAM in the preceding austral spring. An observational analysis of the lead-lag relationship between the SAM index and DJF SST across 50° – 65° S shows that maximal correlation ($r \approx -0.75$) is attained when SST is lagged by one month. Therefore, we assess the relationship between Southern Ocean SST anomalies in DJF with SAM variability in November–January (NDJ) in the CESM1-LE. To isolate the effect of internal

variability, we evaluate the variance of SAM and Southern Ocean SST after removing the ensemble-mean values, which represent the responses to anthropogenic forcing.

Though rare, abrupt Southern Ocean warming events like those observed in late 2016 and 2019 appear in the CESM1-LE (Figs. 8a,b). In the CESM1-LE, NDJ periods where the SAM index is more than 1.5 standard deviations below average occur roughly once every 20 years. The distribution of NDJ SAM events also has a notable skew toward negative SAM events (Fig. 8a). Importantly, the simulated Southern Ocean SST and MLD responses to late-spring SAM variability are consistent with observations. In particular, the anomalous mixed layer warming and shoaling observed in late 2016 and 2019 are similar in magnitude to those produced by comparable SAM events in the CESM1-LE (Figs. 8c,d).

In the observational record, strong SAM and ENSO events sometimes co-occur (e.g., during the austral spring of 1982 and 2002; Fig. 2), which makes it difficult to separate their effects. To quantify the relative effect of SAM and ENSO in the CESM1-LE, we create composites of Southern Ocean SST and MLD anomalies using 0.5 standard deviation bins.

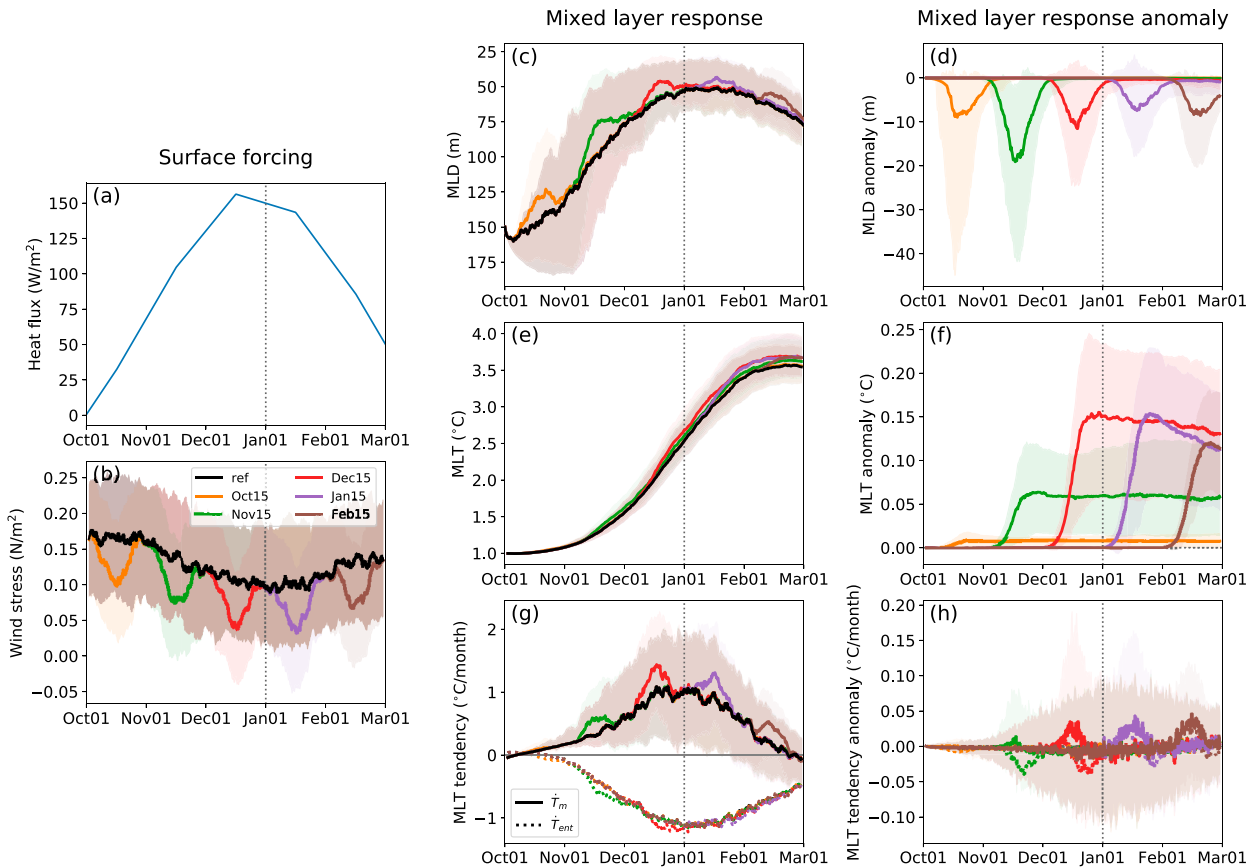


FIG. 6. Results from the idealized 1D mixing experiments: (a) The prescribed surface heat fluxes used in all experiments. (b) The surface wind stress magnitude for the reference and perturbation experiments. For the perturbation runs, a Gaussian filter was used to dampen the winds by a maximum of 25% over a 10-day window centered on the midpoint of each month between October and February. The (c) MLD, (e) MLT, and (g) MLT tendency responses, and (d),(f),(h) the mixed layer response anomalies relative to the reference case with no wind perturbation. Each experiment consists of 500 ensemble members forced by a unique wind time series constructed from a red noise spectrum. The shading represents the interquartile range, and solid lines represent the median response. In (g) and (h), dotted lines represent mixed layer temperature tendency associated with entrainment \dot{T}_{ent} . The interquartile range for \dot{T}_{ent} is omitted for clarity. See the [appendix](#) and [section 3d](#) for further details.

While ENSO affects Southern Ocean SST via atmospheric teleconnections, this signal is communicated on subseasonal time scales and can influence regional SST on similar time scales as SAM (Li et al. 2021). In the CESM1-LE, SAM has the dominant control over domain-averaged SST and MLD anomalies across 50°–65°S during austral spring and summer. The sensitivity of summertime Southern Ocean SST and MLD to SAM variability is less apparent for individual ensemble members, and a robust dependence on SAM only emerges after averaging anomalies across the 40-member ensemble.

4. Discussion

This study demonstrates that the seasonal phasing of MLD shoaling and air–sea heat fluxes is a key driver of interannual summertime SST variability in the Southern Ocean. Between September and December, the zonally averaged MLD between 50° and 65°S shoals from its winter maximum of ~150 m to its summer minimum of ~50 m (Fig. 5). The rate at which

this shoaling occurs varies substantially from year to year and produces an equivalently large spread in the rate at which the mixed layer warms. In the austral spring of 2016 and 2019, the Southern Ocean mixed layer shoaled at the fastest rates observed during the Argo era, which amplified the warming effect of solar insolation when it was near its seasonal maximum. During both events, the anomalous MLD shoaling was initiated by a dramatic weakening of the circumpolar westerlies associated with strong negative SAM events. The weaker westerlies also reduced northward Ekman transport, further amplifying the mixed layer warming.

While several studies have shown that SAM has substantial control over MLD and MLT (e.g., Sen Gupta and England 2006; Sallée et al. 2010), this study quantifies the degree to which mixed layer warming is sensitive to the timing of SAM events. In particular, a sustained negative SAM event during November–February is expected to yield surface warming anomalies several times larger than that produced by a similar SAM event in October or earlier. The late 2016 and 2019

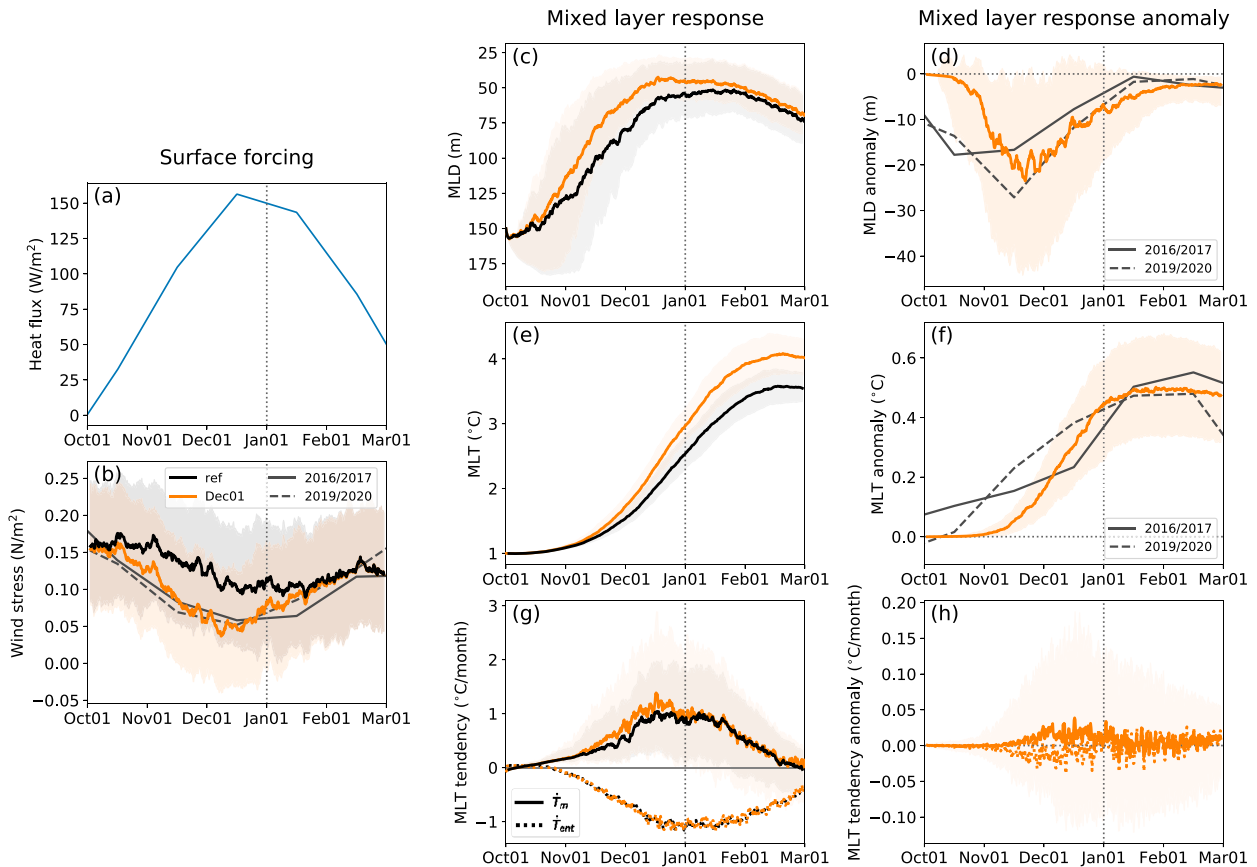


FIG. 7. As in Fig. 6, but showing comparisons for a 50-day wind perturbation experiment centered on 15 Nov. For reference, the observed wind stress and anomalies in MLD and MLT for 2016/17 (solid gray curve) and 2019/20 (dashed gray curve) are shown in (b), (d) and (f), respectively.

warming events followed intense periods of negative SAM, which peaked during November and December, during which the MLT response to surface wind variability is almost maximal. This temporal sensitivity helps to explain why the negative SAM event in late 2002 led to relatively muted surface warming (Figs. 1a and 2c). Although the late 2002 negative SAM event was as intense and prolonged as the 2016 and 2019 SAM events, the former peaked in October before transitioning to a more neutral state in November. Conversely, the timing of the negative SAM events in late 1982 is consistent with the exceptionally strong warming observed that spring (Figs. 1a and 2c).

Abrupt circumpolar surface warming events, such as those observed across the Southern Ocean in late 2016 and 2019, occur in the CESM1-LE roughly every 20 years. In the large ensemble simulations, the Southern Ocean SST and MLD response to SAM aligns well with recent observations. The CESM1-LE also features springtime negative SAM events that are more extreme than what has been observed over the past four decades, suggesting that the SAM variability can drive even more intense summertime surface warming. In the CESM1-LE, SAM has a much stronger influence on zonally averaged summertime SST variability across the circumpolar channel than ENSO. However, examining individual ensemble

members reveals that ENSO and other modes of variability can substantially modulate summertime Southern Ocean SST variability in a given year. Nevertheless, we conclude that the anomalous circumpolar warmings of late 2016 and 2019 were primarily manifestations of internal climate variability. This assessment is in agreement with previous analyses that attribute the sharp decline in Antarctic SIE in late 2016 to internal variability (e.g., Stuecker et al. 2017; Eayrs et al. 2021).

As the circumpolar westerlies continue to intensify and shift poleward, the upper overturning cell of the Southern Ocean is expected to strengthen, increasing the upwelling of warm Circumpolar Deep Water across the Antarctic sea ice zone (Ferreira et al. 2015; Kostov et al. 2017). Stronger winds will likely energize eddies across the circumpolar channel that will partially negate the Ekman overturning response (Farneti et al. 2010; Doddridge et al. 2019). Warming associated with these overturning adjustments may be significant if, as expected, they persist over interannual to decadal time scales. There is evidence that upper ocean upwelling trends have contributed to the below-average Antarctic SIE that has persisted since 2016 (Meehl et al. 2019). The decline in Antarctic sea ice cover over this period is most pronounced in the Weddell Sea (Parkinson 2019), which featured large open-ocean polynyas and deep convection during the winters of 2016

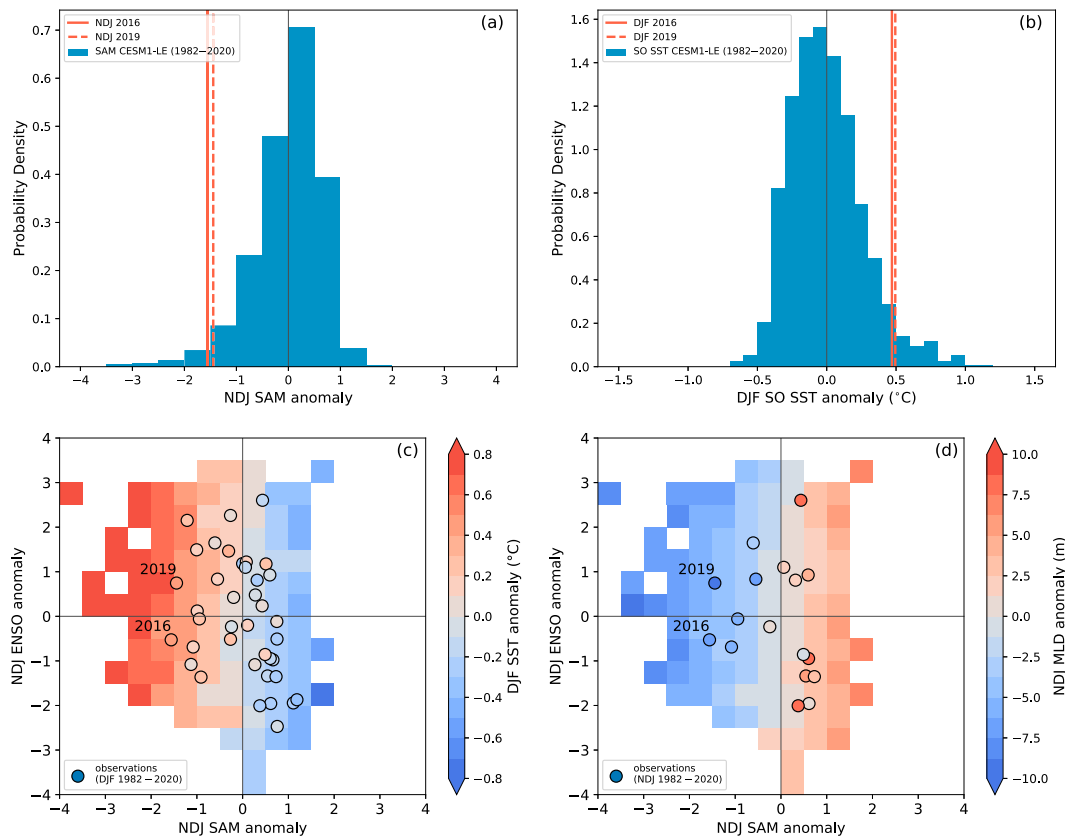


FIG. 8. Comparisons of SAM and Southern Ocean SST variability in the 40-member CESM1-LE with observations for 1982–2020. (a) Probability density distribution of the November–January (NDJ) SAM index in the CESM1-LE. (b) As in (a), but for domain-averaged DJF Southern Ocean SST anomalies across 50° – 65° S. (c) Composites of domain-averaged DJF Southern Ocean SST anomalies in relation to NDJ SAM and ENSO. (d) As in (c), but showing NDJ Southern Ocean MLD anomalies. For the CESM1-LE results, anomalies refer to deviations from the ensemble mean. In (a) and (b), the frequency distributions of SAM and Southern Ocean SST are generated using 0.5 standard deviations and 0.1°C bins, respectively. For the observed seasonal averages shown here, the listed year represents the year the season begins.

and 2017 (Cheon and Gordon 2019). These polynya events were facilitated by enhanced upwelling across the Weddell Gyre, which gradually eroded the local pycnocline and preconditioned the region for deep convection (Campbell et al. 2019). Thus, we surmise that the anomalous Southern Ocean surface warming and sea ice loss since 2016 has been due to a culmination of several climate processes acting over subseasonal to interannual time scales.

Additional work is needed to determine how the variability of SAM and its impacts on Southern Ocean MLD and SST will evolve under anthropogenic forcing. Previous studies have primarily focused on the mean-state ocean response to the ongoing trend toward a more positive SAM phase, in particular, the ocean overturning adjustment to a strengthening and poleward shift of the circumpolar westerlies (e.g., Bitz and Polvani 2012; Ferreira et al. 2015; Kostov et al. 2017). However, our results demonstrate that near-surface processes acting on subseasonal time scales will play a key role in setting future surface warming extremes. While the current positive trend in the SAM index favors more vigorous wind-driven

mixing and deeper mixed layers, concurrent surface warming and freshening trends favor stronger near-surface stratification and possibly shallower mixed layers (Panassa et al. 2018). These competing processes have deepened the Southern Ocean mixed layer and strengthened the upper ocean stratification (Sallée et al. 2021). The extent to which these trends persist will impact the frequency and intensity of future abrupt surface warming events and marine heatwaves in the Southern Ocean.

The evolving seasonality of SAM will likely influence the occurrence of extreme warming events in the Southern Ocean. Recent SAM trends have been attributed to stratospheric ozone depletion, which favors a strengthening and poleward shift of circumpolar westerlies during austral summer (Thompson and Solomon 2002; Polvani et al. 2011). As the stratospheric ozone levels recover, these seasonal SAM trends are expected to subside and possibly reverse (Solomon et al. 2016; Banerjee et al. 2020). Separately, the increase in greenhouse gas concentrations will contribute to a strengthening of the circumpolar westerlies, but the extent to which this effect will negate the ozone-induced SAM trends is unclear. Nevertheless, if the Antarctic ozone

hole recovery continues, the ensuing reduction in positive SAM anomalies in austral summer will favor more extreme surface warming events during these months.

5. Conclusions

The abrupt Southern Ocean surface warming events of late 2016 and 2019 were primarily caused by amplified air–sea heating and reduced northward Ekman transport. The former effect was caused by an unusually early springtime shoaling of the Southern Ocean mixed layer. Both surface warming events were initiated by a severe weakening of the circumpolar westerlies associated with extreme negative SAM events. Equivalent warming events are found in the CESM1-LE, wherein the Southern Ocean SST and MLD response to SAM are consistent with recent observations. Therefore, it is plausible that recent Southern Ocean surface warming anomalies were largely the result of internal variability. A key insight from this analysis is that the Southern Ocean SST response is highly sensitive to the timing of SAM anomalies, with negative SAM anomalies in late spring providing the strongest surface warming. By examining the upper ocean processes that can produce extreme circumpolar summertime warming, we have shed light on the processes that help establish the upper bound of surface temperatures that may occur in the Southern Ocean.

This work mainly elucidates mechanisms that can lead to extreme circumpolar summertime warming across the Southern Ocean. Additional processes operating on smaller spatial scales, such as mesoscale and submesoscale processes (Gao et al. 2022; du Plessis et al. 2022), may augment large-scale warming patterns and create more severe local SST extremes. Moreover, the mixed layer response to SAM has strong interbasin asymmetries, featuring a prominent dipole MLT anomaly across the eastern Pacific and western Atlantic (Sen Gupta and England 2006; Sallée et al. 2010). Although these smaller-scale processes and features are critically important for understanding regional warming patterns, we emphasize that the warming mechanisms we explore in this study, specifically the MLD response to wind perturbations in austral spring, operate across all spatial scales and will contribute to local warming patterns. Further work is also needed to examine how these abrupt summertime warming events may impact upper ocean processes in subsequent seasons. Previous work has shown that strong summertime winds may reduce Antarctic SIE the following winter, whereby enhanced wind-driven mixing in the summer causes an increase in ocean heat uptake that is released during the fall (Doddrige et al. 2021). Therefore, it is plausible that anomalously weak summertime winds could impact subsequent sea ice growth via a similar mechanism.

As the Southern Ocean climate evolves over the twenty-first century, the frequency and intensity of surface warming extremes will depend on the evolution of SAM, surface winds, and MLD. Although past studies have shown the current trend toward positive SAM will eventually lead to sustained surface warming across the Southern Ocean (Ferreira et al. 2015; Bitz and Polvani 2012), it is less clear how the interannual variability of SAM and summertime Southern Ocean SST will coevolve. The severity of future surface warming events in the Southern

Ocean will partly depend on the evolution of the regional MLD; if the springtime MLD shoals over the next century, this will favor more intense summertime warming events. Projecting the evolution of Southern Ocean MLD is complicated by its dependence on competing processes: the projected strengthening of the circumpolar westerlies and increases in surface buoyancy fluxes via warming and enhanced freshwater fluxes (Meredith et al. 2022; Sallée et al. 2021). In a scenario where stronger winds dominate MLD trends, the Southern Ocean surface may experience steady decadal warming but reduced interannual variability due to a concurrent deepening of the mixed layer in spring and summer. Alternatively, if the surface mixed layer shoals over the coming decades, the region will likely experience more intense surface warming extremes, which would exacerbate the impact of the expected time-mean surface warming trend. These extreme warming scenarios will have profound consequences for the viability of regional ecosystems and biogeochemical processes. Thus, it is critical to establish bounds on the temporal variance that may envelope future warming trends.

Acknowledgments. E.A.W. acknowledges support from Caltech's Terrestrial Hazard Observations and Reporting Center. D.B.B. was supported by the National Science Foundation Graduate Research Fellowship Program (NSF Grant DGE-1745301). A.F.T. received support from NSF Award OCE-1756956 and the Internal Research and Technology Development program (Earth 2050), Jet Propulsion Laboratory, California Institute of Technology. E.A.W. and S.C.R. received support through the SOCCOM Project, funded by the National Science Foundation, Division of Polar Programs (NSF PLR-1425989 and OPP-1936222). E.A.W. and S.C.R. also received funding from NOAA as part of the U.S. Argo Program via Grant NA20OAR4320271 to the University of Washington. We thank Edward Doddrige and an anonymous referee for insightful feedback that substantially improved the quality of this manuscript.

Data availability statement. All data and reanalysis products used in this study are sourced from publicly accessible repositories. NOAA Optimum Interpolation SST V2 data were retrieved from <https://psl.noaa.gov/data/gridded/data.noaa.oisst.v2.html>. The Roemmich-Gilson Argo product was downloaded from https://sio-argo.ucsd.edu/RG_Climatology.html. ERA5 reanalysis can be accessed at <https://doi.org/10.24381/cds.f17050d7>. Model output from the CESM1-LE can be downloaded from <https://www.cesm.ucar.edu/projects/community-projects/LENS/data-sets.html>. NOAA/NSIDC Climate Data Record of Passive Microwave Sea Ice Concentration (Version 4) can be accessed at <https://doi.org/10.7265/efmz-2t65>. Python code for carrying out analysis and generating figures is available at <https://doi.org/10.5281/zenodo.6588645>.

APPENDIX

Ensemble Experiments with a 1D Mixing Model

To evaluate the impact of wind perturbations on MLT warming, we use a modified version of the Kraus–Turner 1D upper ocean mixing model (Kraus and Turner 1967; Niiler 1975; Niiler

and Kraus 1977). This bulk mixed layer model simulates the evolution of the surface mixed layer by balancing the stabilizing effect of surface buoyancy fluxes (i.e., the addition of heat or freshwater to the water column) and the destabilizing effect of wind-driven mixing. Variants of the Kraus–Turner model have been used extensively to study surface mixed layer variations over a wide range of settings, including in subpolar regions (Biddle et al. 2017). Following Chen et al. (1994), the entrainment rate w_{ent} of the mixed layer is given by

$$w_{\text{ent}} = \frac{P_w - P_b}{h_m \Delta b}, \quad (\text{A1})$$

where Δb is the buoyancy difference across the base of the mixed layer, and P_w and P_b are work provided by surface wind stress and the potential energy supplied by surface buoyancy fluxes, respectively. The terms P_w and P_b are given by

$$P_w = 2\gamma_1 u_*^3, \quad (\text{A2})$$

$$P_b = \frac{h_m}{2} [(1 + \gamma_2)B_0 - (1 - \gamma_2)|B_0|], \quad (\text{A3})$$

where $\gamma_1 = 0.4$ and $\gamma_2 = 0.18$ are empirically derived mixing coefficients, $u_* = \sqrt{\tau^x/\rho_0}$ is the friction velocity, and B_0 is the total surface buoyancy flux. The above formulation is valid for a stably stratified water column ($\Delta b > 0$). For scenarios where $P_w - P_b > 0$, the mixed layer deepens and (A1) is used to determine the entrainment rate. For cases of mixed layer shoaling, we assume P_w and P_b are in balance, and we use the relationships (A2) and (A3) to determine h_m .

The model is augmented with a parameterization of northward Ekman transport, which introduces a mixed layer cooling given by

$$\dot{T}_{\text{EK}} = -v_{\text{EK}} \frac{\partial T_m}{\partial y}, \quad (\text{A4})$$

where $v_{\text{EK}} = \tau^x/(\rho_0 f h_m)$. For simplicity, we set $\partial T_m/\partial y = 4.5 \times 10^{-6} \text{ }^\circ\text{C m}^{-1}$, which is approximately the annual mean meridional MLT gradient across 50° – 65°S .

The mixing model is initialized with idealized temperature and salinity profiles representative of the circumpolar channel between 50° and 65°S in early October. At the start of each simulation, the mixed layer depth is set to 150 m, and temperature and salinity in the mixed layer are set to 1°C and 33.4 psu, respectively. Below the mixed layer, there is a 150-m-thick seasonal pycnocline, across which temperature and salinity linearly transition to fixed values of 2.5°C and ~ 34.3 psu, respectively. The values at the base of the pycnocline represent the top of the Circumpolar Deep Water layer. We prescribe a surface heat flux that approximates the climatological net surface heating across the circumpolar channel between October and March (150 days total). To isolate the impact of surface winds and heating, we impose a constant surface freshwater flux (i.e., precipitation minus evaporation) of 4 mm day^{-1} . The buoyancy forcing is combined with a synthetically generated surface wind stress τ , which is modeled as the sum of a red-noise sequence $\hat{\tau}(t)$ and a mean offset $\bar{\tau}$:

$$\tau(t) = \hat{\tau}(t) + \bar{\tau}, \quad (\text{A5})$$

$$\hat{\tau}(t) = a\hat{\tau}(t - \Delta t) + \sqrt{(1 - a^2)}\epsilon(t), \quad (\text{A6})$$

where $a = 0.9$ is the lag-1 autocorrelation coefficient, $\Delta t = 6 \text{ h}$ is the time step, and ϵ is a randomly generated white noise sequence with a standard deviation of 0.15 N m^{-2} . The monthly mean offset $\bar{\tau}$ is set by the climatology computed from ERA reanalysis, which decreases from 0.17 N m^{-2} in October to 0.1 N m^{-2} in December. The numerical model is evolved with a vertical resolution of 1 m and a 6-hourly time step.

For the wind perturbation experiments, the magnitude of the time-mean wind stress is altered by a prescribed fraction. By perturbing $\bar{\tau}$ in Eq. (A6), the temporal variance of τ is preserved.

REFERENCES

- Abernathey, R. P., I. Cerovecki, P. R. Holland, E. Newsom, M. Mazloff, and L. D. Talley, 2016: Water-mass transformation by sea ice in the upper branch of the Southern Ocean overturning. *Nat. Geosci.*, **9**, 596–601, <https://doi.org/10.1038/ngeo2749>.
- Armour, K. C., J. Marshall, J. R. Scott, A. Donohoe, and E. R. Newsom, 2016: Southern Ocean warming delayed by circumpolar upwelling and equatorward transport. *Nat. Geosci.*, **9**, 549–554, <https://doi.org/10.1038/ngeo2731>.
- Banerjee, A., J. C. Fyfe, L. M. Polvani, D. Waugh, and K.-L. Chang, 2020: A pause in Southern Hemisphere circulation trends due to the Montreal Protocol. *Nature*, **579**, 544–548, <https://doi.org/10.1038/s41586-020-2120-4>.
- Biddle, L. C., K. J. Heywood, J. Kaiser, and A. Jenkins, 2017: Glacial meltwater identification in the Amundsen Sea. *J. Phys. Oceanogr.*, **47**, 933–954, <https://doi.org/10.1175/JPO-D-16-0221.1>.
- Bintanja, R., G. J. van Oldenborgh, S. S. Drijfhout, B. Wouters, and C. A. Katsman, 2013: Important role for ocean warming and increased ice-shelf melt in Antarctic sea-ice expansion. *Nat. Geosci.*, **6**, 376–379, <https://doi.org/10.1038/ngeo1767>.
- Bitz, C. M., and L. M. Polvani, 2012: Antarctic climate response to stratospheric ozone depletion in a fine resolution ocean climate model. *Geophys. Res. Lett.*, **39**, L20705, <https://doi.org/10.1029/2012GL053393>.
- Campbell, E. C., E. A. Wilson, G. W. Moore, S. C. Riser, C. E. Brayton, M. R. Mazloff, and L. D. Talley, 2019: Antarctic offshore polynyas linked to Southern Hemisphere climate anomalies. *Nature*, **570**, 319–325, <https://doi.org/10.1038/s41586-019-1294-0>.
- Carranza, M. M., and S. T. Gille, 2015: Southern Ocean wind-driven entrainment enhances satellite chlorophyll-a through the summer. *J. Geophys. Res. Oceans*, **120**, 304–323, <https://doi.org/10.1002/2014JC010203>.
- Cavaliere, D. J., C. L. Parkinson, and K. Y. Vinnikov, 2003: 30-year satellite record reveals contrasting Arctic and Antarctic decadal sea ice variability. *Geophys. Res. Lett.*, **30**, 1970, <https://doi.org/10.1029/2003GL018031>.
- Chen, D., L. M. Rothstein, and A. J. Busalacchi, 1994: A hybrid vertical mixing scheme and its application to tropical ocean models. *J. Phys. Oceanogr.*, **24**, 2156–2179, [https://doi.org/10.1175/1520-0485\(1994\)024<2156:AHVMSA>2.0.CO;2](https://doi.org/10.1175/1520-0485(1994)024<2156:AHVMSA>2.0.CO;2).
- Cheon, W. G., and A. L. Gordon, 2019: Open-ocean polynyas and deep convection in the Southern Ocean. *Sci. Rep.*, **9**, 6935, <https://doi.org/10.1038/s41598-019-43466-2>.

- Chung, E.-S., and Coauthors, 2022: Antarctic sea-ice expansion and Southern Ocean cooling linked to tropical variability. *Nat. Climate Change*, **12**, 461–468, <https://doi.org/10.1038/s41588-022-01339-z>.
- Ciasto, L. M., and M. H. England, 2011: Observed ENSO teleconnections to Southern Ocean SST anomalies diagnosed from a surface mixed layer heat budget. *Geophys. Res. Lett.*, **38**, L09701, <https://doi.org/10.1029/2011GL046895>.
- Danabasoglu, G., S. C. Bates, B. P. Briegleb, S. R. Jayne, M. Jochum, W. G. Large, S. Peacock, and S. G. Yeager, 2012: The CCSM4 ocean component. *J. Climate*, **25**, 1361–1389, <https://doi.org/10.1175/JCLI-D-11-00091.1>.
- de Boyer Montégut, C., G. Madec, A. S. Fischer, A. Lazar, and D. Iudicone, 2004: Mixed layer depth over the global ocean: An examination of profile data and a profile-based climatology. *J. Geophys. Res.*, **109**, C12003, <https://doi.org/10.1029/2004JC002378>.
- Ding, Q., E. J. Steig, D. S. Battisti, and J. M. Wallace, 2012: Influence of the tropics on the Southern Annular Mode. *J. Climate*, **25**, 6330–6348, <https://doi.org/10.1175/JCLI-D-11-00523.1>.
- Doddridge, E. W., and J. Marshall, 2017: Modulation of the seasonal cycle of Antarctic sea ice extent related to the Southern Annular Mode. *Geophys. Res. Lett.*, **44**, 9761–9768, <https://doi.org/10.1002/2017GL074319>.
- , —, H. Song, J.-M. Campin, M. Kelley, and L. Nazarenko, 2019: Eddy compensation dampens Southern Ocean sea surface temperature response to westerly wind trends. *Geophys. Res. Lett.*, **46**, 4365–4377, <https://doi.org/10.1029/2019GL082758>.
- , —, —, —, and —, 2021: Southern Ocean heat storage, reemergence, and winter sea ice decline induced by summertime winds. *J. Climate*, **34**, 1403–1415, <https://doi.org/10.1175/JCLI-D-20-0322.1>.
- Dong, S., S. T. Gille, and J. Sprintall, 2007: An assessment of the Southern Ocean mixed layer heat budget. *J. Climate*, **20**, 4425–4442, <https://doi.org/10.1175/JCLI4259.1>.
- , J. Sprintall, S. T. Gille, and L. Talley, 2008: Southern Ocean mixed-layer depth from Argo float profiles. *J. Geophys. Res.*, **113**, C06013, <https://doi.org/10.1029/2006JC004051>.
- du Plessis, M. D., S. Swart, L. C. Biddle, I. S. Giddy, P. M. S. Monteiro, C. J. C. Reason, A. F. Thompson, and S. Nicholson, 2022: The daily-resolved Southern Ocean mixed layer: Regional contrasts assessed using glider observations. *J. Geophys. Res. Oceans*, **127**, e2021JC017760, <https://doi.org/10.1029/2021JC017760>.
- Eayrs, C., X. Li, M. N. Raphael, and D. M. Holland, 2021: Rapid decline in Antarctic sea ice in recent years hints at future change. *Nat. Geosci.*, **14**, 460–464, <https://doi.org/10.1038/s41561-021-00768-3>.
- Fan, T., C. Deser, and D. P. Schneider, 2014: Recent Antarctic sea ice trends in the context of Southern Ocean surface climate variations since 1950. *Geophys. Res. Lett.*, **41**, 2419–2426, <https://doi.org/10.1002/2014GL059239>.
- Farneti, R., T. L. Delworth, A. J. Rosati, S. M. Griffies, and F. Zeng, 2010: The role of mesoscale eddies in the rectification of the Southern Ocean response to climate change. *J. Phys. Oceanogr.*, **40**, 1539–1557, <https://doi.org/10.1175/2010JPO4353.1>.
- Ferreira, D., J. Marshall, C. M. Bitz, S. Solomon, and A. Plumb, 2015: Antarctic Ocean and sea ice response to ozone depletion: A two-time-scale problem. *J. Climate*, **28**, 1206–1226, <https://doi.org/10.1175/JCLI-D-14-00313.1>.
- Fox-Kemper, B., R. Ferrari, and R. Hallberg, 2008: Parameterization of mixed layer eddies. Part I: Theory and diagnosis. *J. Phys. Oceanogr.*, **38**, 1145–1165, <https://doi.org/10.1175/2007JPO3792.1>.
- Frölicher, T. L., E. M. Fischer, and N. Gruber, 2018: Marine heatwaves under global warming. *Nature*, **560**, 360–364, <https://doi.org/10.1038/s41586-018-0383-9>.
- Gao, Y., I. Kamenkovich, N. Perlin, and B. Kirtman, 2022: Oceanic advection controls mesoscale mixed layer heat budget and air–sea heat exchange in the Southern Ocean. *J. Phys. Oceanogr.*, **52**, 537–555, <https://doi.org/10.1175/JPO-D-21-0063.1>.
- Haumann, F. A., N. Gruber, and M. Münnich, 2020: Sea-ice induced Southern Ocean subsurface warming and surface cooling in a warming climate. *AGU Adv.*, **1**, e2019AV000132, <https://doi.org/10.1029/2019AV000132>.
- Hersbach, H., and Coauthors, 2020: The ERA5 global reanalysis. *Quart. J. Roy. Meteor. Soc.*, **146**, 1999–2049, <https://doi.org/10.1002/qj.3803>.
- Hobday, A. J., and Coauthors, 2016: A hierarchical approach to defining marine heatwaves. *Prog. Oceanogr.*, **141**, 227–238, <https://doi.org/10.1016/j.pocean.2015.12.014>.
- Holbrook, N. J., and Coauthors, 2019: A global assessment of marine heatwaves and their drivers. *Nat. Commun.*, **10**, 2624, <https://doi.org/10.1038/s41467-019-10206-z>.
- Holland, M. M., L. Landrum, Y. Kostov, and J. Marshall, 2017: Sensitivity of Antarctic sea ice to the Southern Annular Mode in coupled climate models. *Climate Dyn.*, **49**, 1813–1831, <https://doi.org/10.1007/s00382-016-3424-9>.
- Huang, C. J., F. Qiao, and D. Dai, 2014: Evaluating CMIP5 simulations of mixed layer depth during summer. *J. Geophys. Res. Oceans*, **119**, 2568–2582, <https://doi.org/10.1002/2013JC009535>.
- Hurrell, J. W., and Coauthors, 2013: The Community Earth System Model: A framework for collaborative research. *Bull. Amer. Meteor. Soc.*, **94**, 1339–1360, <https://doi.org/10.1175/BAMS-D-12-00121.1>.
- Kay, J. E., and Coauthors, 2015: The Community Earth System Model (CESM) large ensemble project: A community resource for studying climate change in the presence of internal climate variability. *Bull. Amer. Meteor. Soc.*, **96**, 1333–1349, <https://doi.org/10.1175/BAMS-D-13-00255.1>.
- Kostov, Y., J. Marshall, U. Hausmann, K. C. Armour, D. Ferreira, and M. M. Holland, 2017: Fast and slow responses of Southern Ocean sea surface temperature to SAM in coupled climate models. *Climate Dyn.*, **48**, 1595–1609, <https://doi.org/10.1007/s00382-016-3162-z>.
- Kraus, E. B., and J. S. Turner, 1967: A one-dimensional model of the seasonal thermocline: II. The general theory and its consequences. *Tellus*, **19**, 98–106, <https://doi.org/10.3402/tellusa.v19i1.9753>.
- Li, X., and Coauthors, 2021: Tropical teleconnection impacts on Antarctic climate changes. *Nat. Rev. Earth Environ.*, **2**, 680–698, <https://doi.org/10.1038/s43017-021-00204-5>.
- Marshall, G. J., 2003: Trends in the Southern Annular Mode from observations and reanalyses. *J. Climate*, **16**, 4134–4143, [https://doi.org/10.1175/1520-0442\(2003\)016<4134:TTSAM>2.0.CO;2](https://doi.org/10.1175/1520-0442(2003)016<4134:TTSAM>2.0.CO;2).
- Meehl, G. A., J. M. Arblaster, C. M. Bitz, C. T. Y. Chung, and H. Teng, 2016: Antarctic sea-ice expansion between 2000 and 2014 driven by tropical Pacific decadal climate variability. *Nat. Geosci.*, **9**, 590–595, <https://doi.org/10.1038/ngeo2751>.
- , —, C. T. Y. Chung, M. M. Holland, A. DuVivier, L. A. Thompson, D. Yang, and C. M. Bitz, 2019: Sustained ocean changes contributed to sudden Antarctic sea ice retreat in late 2016. *Nat. Commun.*, **10**, 14, <https://doi.org/10.1038/s41467-018-07865-9>.
- Meier, W. N., F. Fetterer, A. K. Windnagel, and S. Stewart, 2021: NOAA/NSIDC Climate Data Record of Passive Microwave Sea Ice Concentration, Version 4. Boulder, Colorado USA.

- NSIDC: National Snow and Ice Data Center, accessed 15 December 2021, <https://doi.org/10.7265/efmz-2t65>.
- Meredith, M., and Coauthors, 2022: Polar regions. *Ocean and Cryosphere in a Changing Climate*, H.-O. Pörtner et al., Eds., Cambridge University Press, 203–320, <https://doi.org/10.1017/9781009157964.005>.
- Niiler, P. P., 1975: The deepening of the wind-mixed layer. *J. Mar. Res.*, **33**, 405–422.
- , and E. B. Kraus, 1977: One dimensional models of the upper ocean. *Modelling and Prediction of the Upper Layers of the Ocean*, E. B. Kraus, Ed., Pergamon, 143–172.
- Oliver, E. C. J., J. A. Benthuyens, S. Darmaraki, M. G. Donat, A. J. Hobday, N. J. Holbrook, R. W. Schlegel, and A. Sen Gupta, 2021: Marine heatwaves. *Annu. Rev. Mar. Sci.*, **13**, 313–342, <https://doi.org/10.1146/annurev-marine-032720-095144>.
- Panassa, E., C. Völker, D. Wolf-Gladrow, and J. Hauck, 2018: Drivers of interannual variability of summer mixed layer depth in the Southern Ocean between 2002 and 2011. *J. Geophys. Res. Oceans*, **123**, 5077–5090, <https://doi.org/10.1029/2018JC013901>.
- Parkinson, C. L., 2019: A 40-y record reveals gradual Antarctic sea ice increases followed by decreases at rates far exceeding the rates seen in the Arctic. *Proc. Natl. Acad. Sci. USA*, **116**, 14 414–14 423, <https://doi.org/10.1073/pnas.1906556116>.
- Pellichero, V., J.-B. Sallée, S. Schmidtko, F. Roquet, and J.-B. Charrassin, 2017: The ocean mixed layer under Southern Ocean sea-ice: Seasonal cycle and forcing. *J. Geophys. Res. Oceans*, **122**, 1608–1633, <https://doi.org/10.1002/2016JC011970>.
- Polvani, L. M., D. W. Waugh, G. J. P. Correa, and S.-W. Son, 2011: Stratospheric ozone depletion: The main driver of twentieth-century atmospheric circulation changes in the Southern Hemisphere. *J. Climate*, **24**, 795–812, <https://doi.org/10.1175/2010JCLI3772.1>.
- Purich, A., and M. H. England, 2019: Tropical teleconnections to Antarctic sea ice during austral spring 2016 in coupled pacemaker experiments. *Geophys. Res. Lett.*, **46**, 6848–6858, <https://doi.org/10.1029/2019GL082671>.
- , —, W. Cai, A. Sullivan, and P. J. Durack, 2018: Impacts of broad-scale surface freshening of the Southern Ocean in a coupled climate model. *J. Climate*, **31**, 2613–2632, <https://doi.org/10.1175/JCLI-D-17-0092.1>.
- Rackow, T., S. Danilov, H. F. Goessling, H. H. Hellmer, D. V. Sein, T. Semmler, D. Sidorenko, and T. Jung, 2022: Delayed Antarctic sea-ice decline in high-resolution climate change simulations. *Nat. Commun.*, **13**, 637, <https://doi.org/10.1038/s41467-022-28259-y>.
- Reynolds, R. W., N. A. Rayner, T. M. Smith, D. C. Stokes, and W. Wang, 2002: An improved in situ and satellite SST analysis for climate. *J. Climate*, **15**, 1609–1625, [https://doi.org/10.1175/1520-0442\(2002\)015<1609:AIISAS>2.0.CO;2](https://doi.org/10.1175/1520-0442(2002)015<1609:AIISAS>2.0.CO;2).
- Roemmich, D., and J. Gilson, 2009: The 2004–2008 mean and annual cycle of temperature, salinity, and steric height in the global ocean from the Argo Program. *Prog. Oceanogr.*, **82**, 81–100, <https://doi.org/10.1016/j.pcean.2009.03.004>.
- Sallée, J. B., K. G. Speer, and S. R. Rintoul, 2010: Zonally asymmetric response of the Southern Ocean mixed-layer depth to the Southern Annular Mode. *Nat. Geosci.*, **3**, 273–279, <https://doi.org/10.1038/ngeo812>.
- , E. Shuckburgh, N. Bruneau, A. J. S. Meijers, T. J. Bracegirdle, and Z. Wang, 2013: Assessment of Southern Ocean mixed-layer depths in CMIP5 models: Historical bias and forcing response. *J. Geophys. Res. Oceans*, **118**, 1845–1862, <https://doi.org/10.1002/jgrc.20157>.
- Sallée, J.-B., and Coauthors, 2021: Summertime increases in upper-ocean stratification and mixed-layer depth. *Nature*, **591**, 592–598, <https://doi.org/10.1038/s41586-021-03303-x>.
- Schlosser, E., F. A. Haumann, and M. N. Raphael, 2018: Atmospheric influences on the anomalous 2016 Antarctic sea ice decay. *Cryosphere*, **12**, 1103–1119, <https://doi.org/10.5194/tc-12-1103-2018>.
- Sen Gupta, A., and M. H. England, 2006: Coupled ocean-atmosphere-ice response to variations in the Southern Annular Mode. *J. Climate*, **19**, 4457–4486, <https://doi.org/10.1175/JCLI3843.1>.
- Simmonds, I., 2015: Comparing and contrasting the behaviour of Arctic and Antarctic sea ice over the 35 year period 1979–2013. *Ann. Glaciol.*, **56**, 18–28, <https://doi.org/10.3189/2015AoG69A909>.
- Smale, D. A., and Coauthors, 2019: Marine heatwaves threaten global biodiversity and the provision of ecosystem services. *Nat. Climate Change*, **9**, 306–312, <https://doi.org/10.1038/s41558-019-0412-1>.
- Solomon, S., D. J. Ivy, D. Kinnison, M. J. Mills, R. R. Neely III, and A. Schmidt, 2016: Emergence of healing in the Antarctic ozone layer. *Science*, **353**, 269–274, <https://doi.org/10.1126/science.aae0061>.
- Stuecker, M. F., C. M. Bitz, and K. C. Armour, 2017: Conditions leading to the unprecedented low Antarctic sea ice extent during the 2016 austral spring season. *Geophys. Res. Lett.*, **44**, 9008–9019, <https://doi.org/10.1002/2017GL074691>.
- Tamsitt, V., L. D. Talley, M. R. Mazloff, and I. Cerovecki, 2016: Zonal variations in the Southern Ocean heat budget. *J. Climate*, **29**, 6563–6579, <https://doi.org/10.1175/JCLI-D-15-0630.1>.
- Thompson, D. W. J., and S. Solomon, 2002: Interpretation of recent Southern Hemisphere climate change. *Science*, **296**, 895–899, <https://doi.org/10.1126/science.1069270>.
- Turner, J., T. Phillips, G. J. Marshall, J. S. Hosking, J. O. Pope, T. J. Bracegirdle, and P. Deb, 2017: Unprecedented spring-time retreat of Antarctic sea ice in 2016. *Geophys. Res. Lett.*, **44**, 6868–6875, <https://doi.org/10.1002/2017GL073656>.
- Wang, G., H. H. Hendon, J. M. Arblaster, E.-P. Lim, S. Abhik, and P. van Rensch, 2019: Compounding tropical and stratospheric forcing of the record low Antarctic sea-ice in 2016. *Nat. Commun.*, **10**, 13, <https://doi.org/10.1038/s41467-018-07689-7>.
- Yuan, X., and D. G. Martinson, 2000: Antarctic sea ice extent variability and its global connectivity. *J. Climate*, **13**, 1697–1717, [https://doi.org/10.1175/1520-0442\(2000\)013<1697:ASIEVA>2.0.CO;2](https://doi.org/10.1175/1520-0442(2000)013<1697:ASIEVA>2.0.CO;2).
- Zhang, L., T. L. Delworth, W. Cooke, and X. Yang, 2019: Natural variability of Southern Ocean convection as a driver of observed climate trends. *Nat. Climate Change*, **9**, 59–65, <https://doi.org/10.1038/s41558-018-0350-3>.
- , —, X. Yang, F. Zeng, F. Lu, Y. Morioka, and M. Bushuk, 2022: The relative role of the subsurface Southern Ocean in driving negative Antarctic sea ice extent anomalies in 2016–2021. *Commun. Earth Environ.*, **3**, 302, <https://doi.org/10.1038/s43247-022-00624-1>.
- Zheng, X.-T., C. Hui, and S.-W. Yeh, 2018: Response of ENSO amplitude to global warming in CESM large ensemble: Uncertainty due to internal variability. *Climate Dyn.*, **50**, 4019–4035, <https://doi.org/10.1007/s00382-017-3859-7>.